Journal of Theoretical Biology 425 (2017) 1–10

Contents lists available at ScienceDirect

Journal of Theoretical Biology

journal homepage: www.elsevier.com/locate/jtbi

Mathematical model for isometric and isotonic muscle contractions

R. De Vita[a], R. Grange[b], P. Nardinocchi[c,*], L. Teresi[d,e]

[a] STRETCH Laboratory, Department of Biomedical Engineering and Mechanics, Virginia Tech, Blacksburg, VA, 24061, USA
[b] Department of Human Nutrition, Foods, and Exercise, Virginia Tech, Blacksburg, VA, 24061, USA
[c] Dipartimento di Ingegneria Strutturale e Geotecnica, Sapienza Università di Roma, 00184 Roma, Italy
[d] Dipartimento di Matematica e Fisica, Università Roma Tre, 00146 Roma, Italy
[e] LaMS - Modeling & Simulation Lab, Università Roma Tre, 00146 Roma, Italy

ARTICLE INFO

Article history:
Received 25 November 2016
Revised 13 April 2017
Accepted 4 May 2017
Available online 5 May 2017

Keywords:
Continuum mechanics
Muscle modeling
Active strain
Isometric contraction
Isotonic contraction

ABSTRACT

A new mathematical model is presented to describe both the active and passive mechanics of muscles. In order to account for the active response, a two–layer kinematics that introduces both the visible and rest lengths of the muscle is presented within a rational mechanics framework. The formulation is based on an extended version of the principle of virtual power and the dissipation principle. By using an accurate constitutive description of muscle mobility under activation, details of microscopic processes that lead to muscle contraction are glossed over while macroscopic effects of chemical/electrical stimuli on muscle mechanics are retained. The model predictions are tested with isometric and isotonic experimental data collected from murine extensor digitorum muscle. It is shown that the proposed model captures experimental observations with only three scalar parameters.

1. Introduction

Muscle is an active biological material that undergoes large deformations and produces large forces in response to electrical/chemical stimulation. Because of the remarkable mechanical properties of this material, several attempts have been made over the past century to model its active response, starting from Hill's pioneering work (Hill, 1938). Typically, existing models combine different descriptions of the muscle electrophysiological activity occurring at the cellular level, with mechanical models that are formulated within the context of rational continuum mechanics using either the active-passive additive decomposition of the stress response or the active-passive multiplicative decomposition of the deformation gradient (Cherubini et al., 2008; Göktepe et al., 2014; Hunter et al., 1998; Murtada and Holzapfel, 2014; Nardinocchi and Teresi, 2013; Sharifimajd and Stålhand, 2014; Stålhand et al., 2008; 2011; 2016). In both cases, electro-mechano-transduction is modeled by introducing an electrophysiologically-based response function of either the active stress or the active strain of the muscle. Despite these attempts, the ability of muscles to change shape under no force, driving a global shape change of the tissue, still poses unique modeling challenges that are far from being resolved.

Within a purely mechanical model, the details of the muscle electrophysiology can be disregarded as long as the effects on the mechanical response are considered. Following this approach, a model for the active and passive mechanical behavior of biological tissues has been proposed by some of the Authors (Tan and De Vita, 2015). Specifically, within the framework of Hill's three-element model, an evolution law for the deformation of smooth muscle cells and connected collagen fibers is formulated and a contraction force is introduced. This latter is assumed to be the sum of a motor force, describing the actin-myosin filament sliding, and an elastic force that accounts for the cross-bridge deformation. The motor force initiates the contraction of muscle cells, and is identified through a fitting procedure to uniaxial isometric length-tension experimental data (Murtada et al., 2012) and isotonic quick-release experimental data (Dillon et al., 1981) on pig carotid arteries and biaxial isometric inflation-extension experimental data on pig coronary arteries (Chen et al., 2013).

A similar approach is adopted in this manuscript where a model for muscle mechanics is presented. The model has the following main characteristics. It is set within a rational mechanical framework; it accounts for the effect of the electrophysiological input on the mechanical response; and it requires only three scalar parameters (i.e., κ, $\bar{m}$, and $\bar{a}$, related to muscle stiffness, mobility, and activation) to capture the common mechanical response of the muscle under both isometric and isotonic conditions. Ultimately, this model can be used to investigate how biochemical inputs influence mechanical outputs of the muscle.

* Corresponding author.
E-mail addresses: devita@vt.edu (R. De Vita), rgrange@vt.edu (R. Grange), paola.nardinocchi@uniroma1.it (P. Nardinocchi), teresi@uniroma3.it (L. Teresi).

http://dx.doi.org/10.1016/j.jtbi.2017.05.007
0022-5193/

The model is formulated within the rational mechanics framework set forth by Rodriguez et al. (1994) and formalized by DiCarlo and Quiligotti (2002). Muscle contraction is viewed as a remodeling of the muscle internal structure, i.e. a macroscopic evolution of the rest state of the muscle due to microscopic processes. In order to keep the model as simple as possible, we present a zero-dimensional version, the muscle is viewed as an one-dimensional homogeneous bar. We consider a two layer kinematics which distinguishes muscle shortening due to active contraction by introducing two length measures: the (visible, or experimentally measurable) length and the rest length. This richer kinematics leads to a balance of remodeling force that governs the evolution of the rest length, independently of the balance of standard force. Just as the standard force balance governs motion, the balance of remodeling force governs muscle active contraction. Within this non-standard balance of force, an Eshelby-like contribution appears that is independent of any specific constitutive assumption on the muscle material behavior. For simplicity, we select the Kirchhoff/Saint–Venant constitutive function that depends only on the elastic stiffness κ.

Muscle contraction can be initiated by chemical/electrical stimuli that cause a change in the intracellular calcium concentration. The mechanical output of these stimuli is represented, within our theory, by a muscle activation force a which is related to the activation potential applied to the muscle during experiments and is parametrized by its intensity $\bar{a}$. On the other hand, we control the muscle electro-physiological characteristics through a function m which accounts, at the macro-scale level, for the muscle mobility. The general form of the mobility function is dictated by physiological considerations and is parametrized via a scalar $\bar{m}$.

The proposed model results in two coupled equations that define an initial value problem. This problem is solved by considering data collected from murine extensor digitorum muscle (EDL), subjected to isometric and isotonic tests. Ultimately, with only three model parameters, κ, $\bar{m}$, and $\bar{a}$, both force over time at fixed length and shortening over time at fixed force are captured.

This paper is organized as follows. In Section 2 isometric and isotonic experiments are described. We present the basic equations of the muscle model and comment on their key characteristics in Section 3; a detailed derivation within the relevant theoretical framework is given in Section 3.4. In Section 4, isometric and isotonic experiments are simulated using the model and the results are compared to the experimental data by tuning the three model parameters. Brief conclusions are presented in Section 5.

2. Isometric and isotonic data

In vitro contractile data used to develop this model were obtained from the Extensor Digitorum Longus (EDL) muscle of an 11 week old mdx (dystrophic) mouse. The EDL muscle (11.6 mm, 13.2 mg) was carefully excised from the mouse anesthetized with a ketamine/xylazine cocktail. 4-O silk suture was tied to the proximal and distal myotendinous junctions (Wolff et al., 2006). The muscle was fixed between the arm of a dual-mode servomotor system (300B, Aurora Scientific) and a clamp positioned at the bottom of the muscle bath filled with an oxygenated (95% O_2, 5% CO_2) physiological salt solution prepared as described previously (Wolff et al., 2006), and maintained at 30 °C. The muscle was pre-loaded to an initial resting force of 1.0 g, which was maintained by a stepper motor; the force and position inputs of the servomotor arm and the stepper motor were controlled by Dynamic Muscle Control software (DMC Version 4.1.6, Aurora Scientific). Muscle was field stimulated in the bath via platinum electrodes that closely flanked the muscle (±0.5 cm) with square pulses of 200 – μs duration at 40 volts delivered from a 701C Electrical Stimulator (Aurora Scientific, Inc.). Simulation frequency and duration were controlled by DMC. The electrodes did not touch the muscle, but were close enough to provide field stimulation through the physiological salt solution.

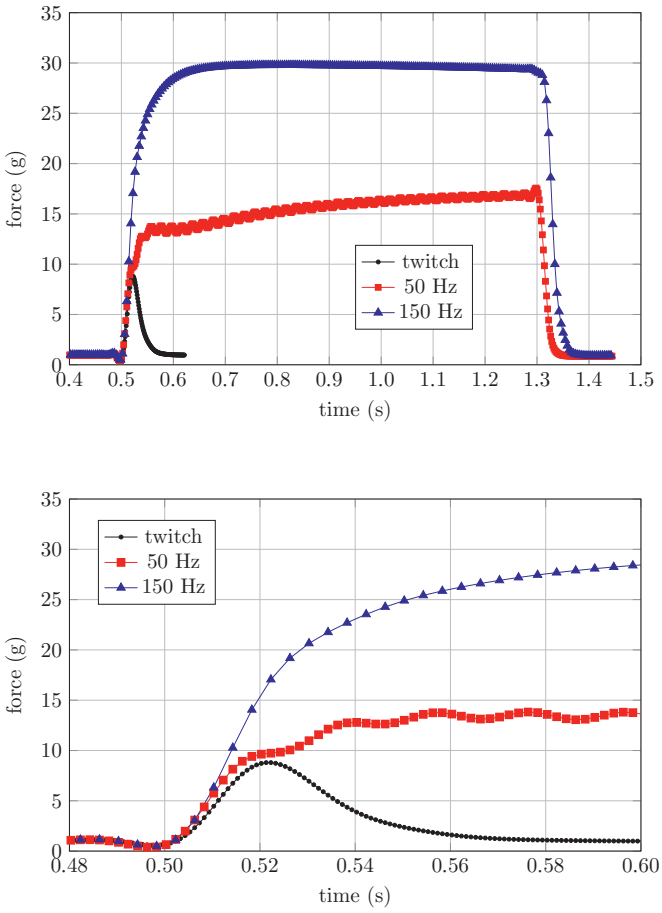

Fig. 1. Results of the isometric experiments for the EDL muscle, obtained with three different stimuli: single twitch; activation frequencies of 50 and 150 Hz as indicated in the plot legend. Top: Force versus time at fixed optimal length. Bottom: Zoomed in view of the top figure with time up to 0.6 s.

The muscle was subjected to isometric contractions at the optimal length $x_o = 11.5$ mm to generate force responses at various activation frequencies: 1, 50, and 150 Hz (1 s duration; 1 min between each contraction) (see Fig. 1). In addition, after a 5 min rest period, the muscle was subjected to activation at 150 Hz to generate isotonic contractions using the tetanic afterload method. Briefly, the muscle was stimulated at 150 Hz at various percentage loads set on the servo motor arm relative to the maximum tetanic force $f^{\max}$ at 150 Hz. The loads included 5, 25, and 75% of maximum tetanic force, each separated by 1 min (see Fig. 2). Details of these contractile property assays can be found in Quiat et al. (2011); Sperringer and Grange (2016). Isometric and isotonic data obtained using the assays described above were used to test the mathematical model.

3. Modeling muscle contraction and relaxation

We identify a prototype muscle with a one-dimensional and homogeneous bar, whose state is described by two variables: one is the (visible) length x and the other one is the rest length x_r ($[x] = [x_r] = L$)[1]. The length x is the experimentally measurable length of the muscle, and does not deserve any further comment. The rest

[1] We use square parenthesis $[\,\cdot\,]$ to denote the physical dimensions of a quantity; L, F, and T are length, force, and time, respectively.

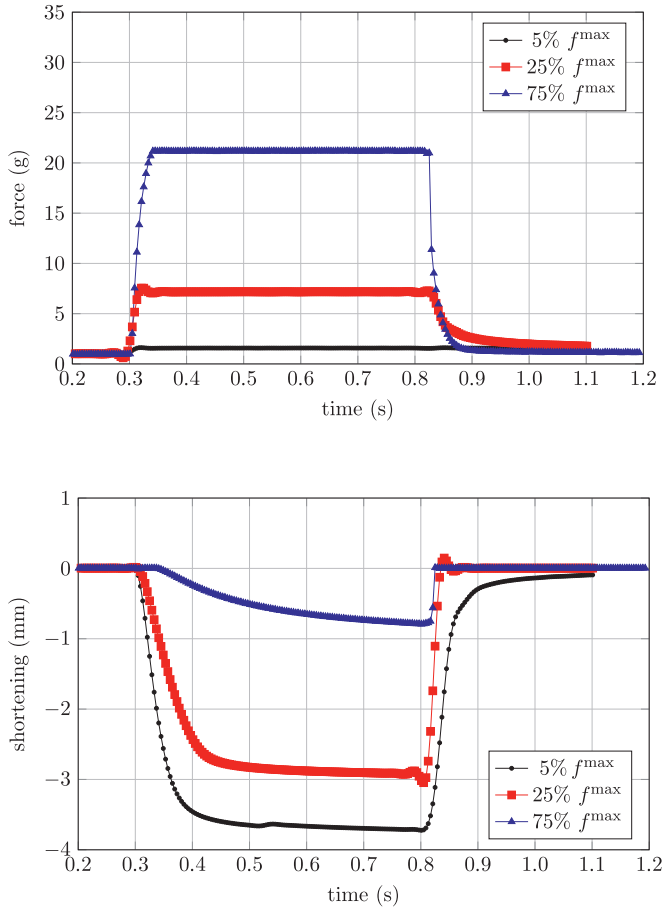

Fig. 2. Results of the isotonic experiments for the EDL muscle. Top: Force versus time at 5, 25, and 75% of the maximum tetanic force f^{max}. Bottom: Shortening versus time.

length x_r is the length in the active or passive state when no external force is applied and cannot be experimentally measured. The term rest length can be used for the entire muscle, as in Fig. 3, or for its subunits; as example, the typical rest length for sarcomeres ranges between 2 μm to 3 μm (Keurs et al., 1980).

The elastic stretch λ_e of the muscle has to be measured with respect to the rest length, and is defined by the following ratio (see Fig. 3)

$$\lambda_e = \frac{x}{x_r}. \tag{1}$$

It is important to note that the activation without the application of a force shortens the muscle, and in this case $x = x_r$ ($\lambda_e = 1$); on the contrary, pulling the muscle without activation lengthens it, causing the same increase in both x and x_r. When a muscle is both activated and loaded, the two effects compete with each other and the muscle is stretched, that is, $x > x_r$ ($\lambda_e > 1$). In this case, a muscle can: i) act as motor: it shortens, lifting a force (activation prevails); ii) act as a brake: it elongates, while sustaining a load (loading prevails) (Dickinson et al., 2000).

We introduce a reference length x_{ref}, and define two further stretches:

$$\lambda = \frac{x}{x_{\text{ref}}}, \quad \lambda_r = \frac{x_r}{x_{\text{ref}}}, \quad \Rightarrow \quad \lambda_e = \frac{x}{x_r} = \frac{\lambda}{\lambda_r}. \tag{2}$$

Moreover, we assume that x_r ranges in $(x_r^{\min}, x_r^{\max})$ and that $x_r^{\min}/x_r^{\max} = 0.6$. The value of this ratio is typical for many different muscles and is strictly linked to the ratio of the minimum and the maximum sarcomere lengths. It is convenient to take the reference length as the maximum rest length, that is $x_{\text{ref}} = x_r^{\max}$. It

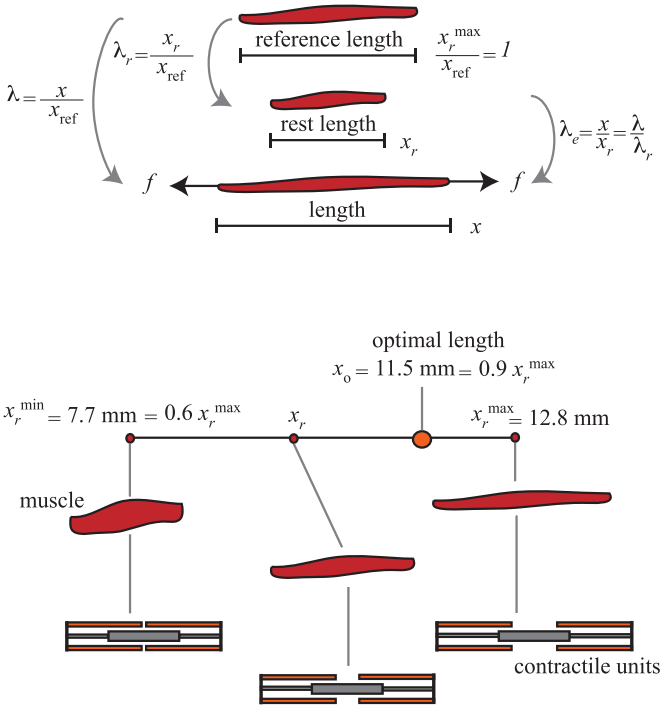

Fig. 3. Length and stretch measures. Top: Stretch measures introduced in the model. Bottom: Typical values of $x_r^{\min}$, $x_r^{\max}$, and x_o (optimal length) for EDL muscle. Note that x_r spans the range $(x_r^{\min}, x_r^{\max})$ (Sperringer and Grange, 2016).

follows that, while λ can, in principle, vary in (0, ∞), λ_r ranges in (0.6,1) (see Fig. 3).

3.1. The evolution equations

The evolution of the state variables (x, x_r) of the model is controlled by two equations, representing the balance of forces and the balance of remodeling forces, a non-standard equation in mechanics, supplemented by initial conditions on x and x_r (DiCarlo and Quiligotti, 2002):

$$f = \sigma, \quad \frac{\dot{x}_r}{x_r} = m(a - \lambda_r e), \tag{3}$$

$$x(0) = x^{\text{init}}, \quad x_r(0) = x_r^{\text{init}}.$$

The above equations describe the *time evolution* of the muscle's state. We consider as inputs for the model the force f, representing the force pulling the muscle, and the activation a, representing the mechanical effects of the electro-physiological stimuli; we note that to obtain a shortening ($\dot{x}_r < 0$), the activation a has to be negative. The output of the model are the state variables x and x_r. Alternatively, we consider as input, in addition to a, a kinematical constraint on x; in this case the outputs are the force f and x_r. In Eq. (3), σ represents the stress, e an Eshelby-like force and $m > 0$ the mobility function ($[f] = [\sigma] = [a] = [e] = F$, $[m] = F^{-1}T^{-1}$).

The term $a - \lambda_r e$ in Eq. $(3)_2$ represents the muscle driving force defined by the competition between activation and force. Its value determines the shortening or lengthening of x_r:

$$\begin{aligned} a - \lambda_r e < 0 \quad &\Rightarrow \quad \dot{x}_r < 0, \quad \text{muscle shortening (motor);} \\ a - \lambda_r e = 0 \quad &\Rightarrow \quad \dot{x}_r = 0, \\ a - \lambda_r e > 0 \quad &\Rightarrow \quad \dot{x}_r > 0, \quad \text{muscle lengthening (brake).} \end{aligned} \tag{4}$$

The stress σ and the Eshelby-like force e are constitutively determined once an energy ψ_r per unit rest length has been selected

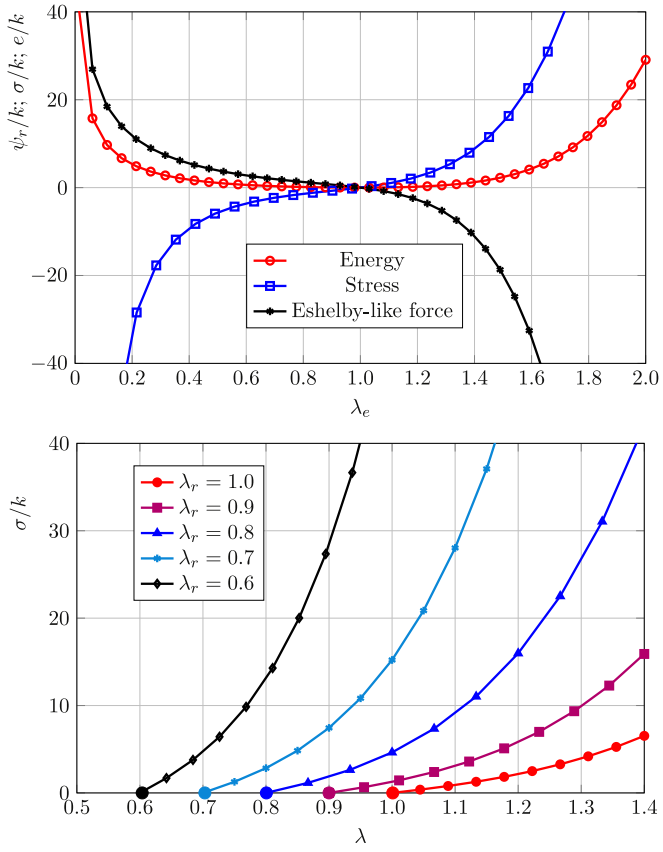

Fig. 4. (top) Dimensionless energy ψ_r/κ, stress σ/κ, and Eshelby-like force e/κ versus elastic strain λ_e. (bottom) Stress σ versus stretch λ for different stretches λ_r.

as a function of the elastic stretch λ_e:

$$\sigma = \hat{\sigma}(\lambda_e) = \psi_r'(\lambda_e)\,, \quad e = \hat{e}(\lambda_e) = \psi_r(\lambda_e) - \lambda_e \psi_r'(\lambda_e)\,, \tag{5}$$

with ψ_r' the derivative of ψ_r with respect to λ_e. Here, for simplicity, we assume ψ_r in the form of a Kirchhof–Saint Venant strain energy

$$\psi_r(\lambda_e) = \frac{1}{8}\kappa(\lambda_e^4 - 1)^2 + \frac{1}{8}\kappa(\log(\lambda_e^4))^2\,, \tag{6}$$

where κ ($[\kappa] = F$) is the elastic stiffness. Fig. 4 (top) shows the dimensionless energy ψ_r/κ, stress σ/κ, and Eshelby-like force e/κ, versus elastic stretch λ_e. We note that the Eshelby-like force is opposite in sign to the stress. It can be shown that, for $\lambda_e = 1 + \varepsilon_e$, $\hat{e}(\varepsilon_e) = -\hat{\sigma}(\varepsilon_e) + o(\varepsilon_e)$; it means that, in a linear theory, where ε_e represents a infinitesimal deformation, the Eshelby-like force is just the opposite of the stress in sign. Fig. 4 (bottom) shows the stress-strain curves for different stretches λ_r that correspond to different rest lengths x_r; given x_{ref}, it can be observed that the elastic response becomes stiffer as x_r decreases, that is, as the muscle contracts. The mobility function m and the activation function a on the right-hand side of Eq. $(3)_2$ bring into the model the electrophysiological characteristics of the muscle. The muscle mobility is determined at the cellular level by the sliding-filament mechanism and by the muscle state. In our model, the mobility function must:

i) define a threshold stress σ_t below which x_r does not change: for $\sigma < \sigma_t$, $\dot{x}_r = 0$, and the response is purely elastic;
ii) maintain the rest length x_r within the physiological limits $x_r^{\min}$ and $x_r^{\max}$;
iii) account for the sign of the muscle driving force $(a - \lambda_r e)$.

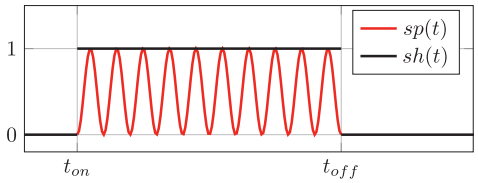

Fig. 5. Functions $sh(t)$ and $sp(t)$ as defined in (10) for $f_r = 10/(t_{\text{off}} - t_{\text{on}})$.

To attain these goals, we assume the mobility m to be a function of $x_r, \sigma - \sigma_t, a - \lambda_r e$:

$$m = m(x_r, \sigma - \sigma_t, a - \lambda_r e)\,,$$

and we define it via the product of two (smoothed) switches as follows:

$$m(x_r, \sigma - \sigma_t, a - \lambda_r e) = \bar{m}\, m_\sigma(\sigma - \sigma_t)\, m_a(x_r, a - \lambda_r e)\,.$$

The function $m_\sigma(\sigma - \sigma_t)$ is introduced to describe item *i*), while the function $m_a(x_r, a - \lambda_r e)$ is introduced to capture items *ii*) and *iii*). Both these functions range in (0, 1), and are defined in terms of the complementary error function $\text{erfc}(x) = 2/\sqrt{\pi}\int_x^\infty \exp(-t^2)\,dt$. Specifically, they have the following form:

$$m_\sigma(\sigma - \sigma_t) = \frac{1}{2}\,\text{erfc}\left(\frac{\delta_\sigma - (\sigma - \sigma_t)}{\sqrt{2}\,\delta_\sigma}\right), \tag{7}$$

and

$$\begin{aligned} &m_a(x_r, a - \lambda_r e) \\ &= \frac{1}{2}\text{erfc}\left(\frac{x_r - (x_r^{\max} - \delta_x)}{\sqrt{2}\,\delta_x/2}\right)\frac{1}{2}\,\text{erfc}\left(\frac{-(a - \lambda_r e)}{\sqrt{2}\delta_a}\right) \\ &+\frac{1}{2}\text{erfc}\left(\frac{-x_r + (x_r^{\min} + \delta_x)}{\sqrt{2}\,\delta_x/2}\right)\frac{1}{2}\,\text{erfc}\left(\frac{a - \lambda_r e}{\sqrt{2}\delta_a}\right). \end{aligned} \tag{8}$$

The parameters $\delta_\sigma = 10^{-3}$, $\delta_x = 2 \cdot 10^{-5}$, and $\delta_a = 8 \cdot 10^{-3}$ in Eqs. (7) and (8) set the smoothness of the transition between 0 and 1; finally, the constant $\bar{m}$ defines the intensity of the mobility.

The function a is related to the activation potential that is applied to the muscle during the experiments: single twitch, summation, and tetanus contractions can be produced based on the frequency of the stimuli. In this coarse description, we will use the following two representations:

$$a(t) = \bar{a}\, sh(t) \quad \text{or} \quad a(t) = \bar{a}\, sp(t)\,, \tag{9}$$

with

$$\begin{aligned} sh(t) &= H(t - t_{\text{on}}) - H(t - t_{\text{off}})\,, \\ sp(t) &= sh(t)\sin^2[(t - t_{\text{on}})\,\pi\, f_r]\,. \end{aligned} \tag{10}$$

Here, $H(\cdot)$ is the Heaviside function, $\bar{a}$ the intensity of the activation, f_r its frequency, and t_{on}, t_{off} the times at which the activation starts and stops, respectively ($[t_{\text{on}}] = [t_{\text{off}}] = T$, $[f_r] = 1/T$). Both these functions are presented in Fig. 5.

As discussed in the next sections, we use $sp(t)$ for modeling the low frequency response (twitch and stimulus at 50 Hz), and $sh(t)$ for the high frequency response (stimulus at 150 Hz, for both isometric and isotonic tests).

3.2. Isometric contractions

An isometric contraction is one in which the muscle is stimulated, producing a force, while its length is kept constant. When the muscle fibers contract, a biophysical process is occurring at a microscopic level; in our model, this process is captured by the change in time of the rest length x_r. The isometric contraction can be described by solving Eqs. (3) under the kinematical constraint

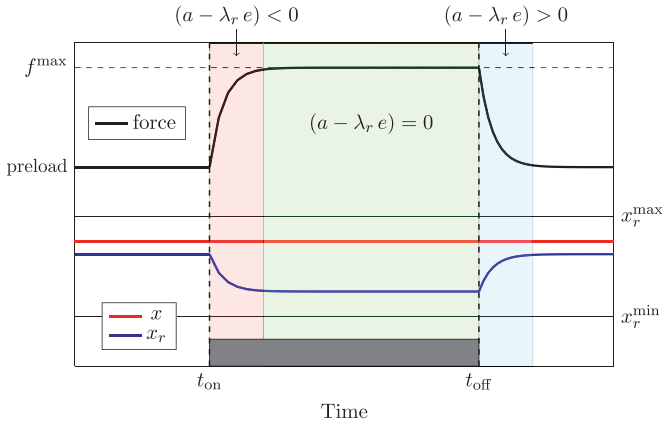

Fig. 6. Isometric contraction. The length x is kept constant. Upon activation at t_{on}, the rest length x_r decreases, and the force increases until it reaches a plateau value when $a-\lambda_r e=0$. At t_{off}, the Eshelby-like term $a-\lambda_r e>0$, where $a=0$, restores the initial rest length while the force decreases to a pre-load value. The dark gray bar denotes the region where the activation is on.

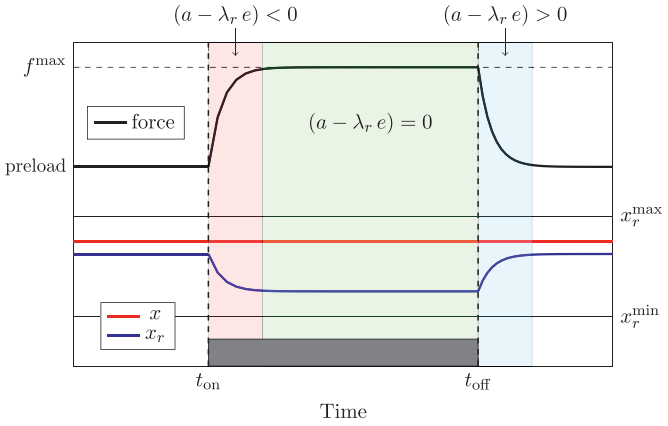

Fig. 7. Isotonic contraction. The force history is controlled. Upon activation at t_{on}, while the force increases until it reaches a plateau value, x_r and x decrease (the muscle acts like a motor) and reach plateau values when $a-\lambda_r e=0$. At t_{off}, the Eshelby-like term $a-\lambda_r e>0$, with $a=0$, causes an increase in x_r and x (muscle acts like a brake) and restores the initial rest length. The dark gray bar denotes the region where the activation is on.

$x=\bar{x}$, where $\bar{x}$ is the constant length at which the experiment is performed. In this case, $\lambda_e=\bar{x}/x_r$, which means that the elastic stretch only depends on the change in x_r. Then, we have

$$f=\hat{\sigma}\left(\frac{\bar{x}}{x_r}\right),\quad \frac{\dot{x}_r}{x_r}=m\left(a-\frac{x_r}{x_{\text{ref}}}\hat{e}\left(\frac{\bar{x}}{x_r}\right)\right),$$

$$x(0)=\bar{x},\quad x_r(0)=\bar{x}-\varepsilon, \tag{11}$$

where ε represents a small change in length due to a pre-stretch applied to the muscle prior to the isometric test. For this problem, the couple $(\bar{x},a)$ is the input, while the couple (x_r, f) is the output. Fig. 6 is a qualitative representation of the results of Eqns. (11). Again, *we note that x_r is a quantity that cannot be measured experimentally.*

We can evaluate the tetanic force $f^{\max}$ that correspond to different constant lengths $\bar{x}$ by solving Eqs. (11) with different inputs $(\bar{x},a)$ and using $sh(t)$ for the activation function. For each value of $\bar{x}$, we compute $f^{\max}$ at the plateau of the force versus time curve; the values of $f^{\max}$ and the corresponding $\bar{x}/x_{\text{ref}}=\bar{\lambda}$ can be used to generate the force-length relationship curve.

3.3. Isotonic contractions

An isotonic muscle contraction is one in which the muscle is stimulated, producing a constant force, while changing its visible length. In our model, this process is described by changes in time of both x and x_r. The isotonic contraction can be described by the solution of Eqs. (3), assigning the couple $(f,\ a)$ as input; in such case $\lambda_e=x/x_r$, which means that the elastic stretch depends on the two state variables. Then, we have

$$f=\hat{\sigma}\left(\frac{x}{x_r}\right),\quad \frac{\dot{x}_r}{x_r}=m\left(a-\frac{x_r}{x_{\text{ref}}}\hat{e}\left(\frac{x}{x_r}\right)\right),$$

$$x(0)=\bar{x},\quad x_r(0)=\bar{x}-\varepsilon. \tag{12}$$

In this case, the couple $(x,\ x_r)$ is the output. The output provides the visible muscle length $x(t)$ under an assigned force history $f(t)$. Fig. 7 is a qualitative representation of the results of Eqs. (12); note that, unlike isometric contractions, the force remains constant even when the activation is off.

3.4. Background: modeling framework

Eqs. (3)are derived within a mechanical framework originally proposed to describe volumetric growth (Rodriguez et al., 1994), that is, changes in shape that do not vary the elastic energy stored in a material (DiCarlo and Quiligotti, 2002). The present model is based on the assumption that the muscles behave in a similar fashion: they change their rest length x_r without varying their elastic energy (Ambrosi et al., 2011; Nardinocchi and Teresi, 2007).

Here we provide a brief, but comprehensive description of the model fundamentals, starting from the *principle of power balance* (Germain, 1972). Given the pair of state variables $(x,\ x_r)$, we define the corresponding pair of velocity and remodeling velocity $(\dot{x},\dot{x}_r/x_r)$; the virtual velocities are then $(\tilde{x},\tilde{x}_r/x_r)$. The principle of power balance says that, for any virtual velocity $(\tilde{x},\tilde{x}_r/x_r)$, the internal power generated by the stress σ on the virtual stretch $\tilde{\lambda}=\tilde{x}/x_{\text{ref}}$ and by the internal remodeling action a^i on $\tilde{x}_r/x_r$ must be equal to the external power generated by the body force p on $\tilde{x}$, by the body external remodeling action a on $\tilde{x}_r/x_r$, and by the force f at the boundary on $\tilde{x}$:

$$\underbrace{\int\left(\sigma\cdot\tilde{\lambda}+a^i\cdot\frac{\tilde{x}_r}{x_r}\right)dx}_{\text{internal power}}=\underbrace{\int\left(p\cdot\tilde{x}+a\cdot\frac{\tilde{x}_r}{x_r}\right)dx+f\cdot\tilde{x}}_{\text{external power}}. \tag{13}$$

The integrals in the above equation are computed with respect to the reference length x_{ref}. All the quantities involved are scalar but we use the dot product symbol to emphasize the duality between kinematics and dynamics.

It is worth noting that, since the internal power is expended by the stress σ on the strain, we have a theory of grade one and we consider both body and boundary forces. On the contrary, for the remodeling actions, we have a theory of grade zero, and boundary remodeling actions cannot be accounted in the model (DiCarlo and Quiligotti, 2002; Minozzi et al., 2015; Nardinocchi and Teresi, 2007; Truesdell, 1965). The assumption of a homogeneous state yields the trivial solution of the integral as:

$$\int(\sigma\cdot\tilde{\lambda})\,dx=(\sigma\cdot\tilde{\lambda})\,x_{\text{ref}}=\sigma\cdot\tilde{x}. \tag{14}$$

We assume that the body force is zero, that is $p=0$. The principle of power balance then yields, for any $\tilde{x}$ and $\tilde{x}_r/x_r$:

$$(\sigma-f)\cdot\tilde{x}=0,\quad (a^i-a)\cdot\frac{\tilde{x}_r}{x_r}=0, \tag{15}$$

that is,

$$\sigma=f,\quad a^i=a. \tag{16}$$

The external remodeling action a and the boundary force f must be considered as input for the model, as they describe the activation and the force sustained by the muscle. We note that quantities similar to a and a^i have been introduced in growth and remodeling theories with various names: configurational forces (Gurtin, 2008), remodeling couples (DiCarlo and Quiligotti, 2002; Nardinocchi and Teresi, 2006), material forces (Maugin, 1993), and accretive forces (Ambrosi and Guana, 2007). The internal remodeling action a^i and the stress σ must be defined by constitutive equations.

The constitutive equations are derived from the *dissipation principle* (Coleman and Noll, 1963): given a free energy ψ per unit of reference-length and denoted with σ^d, a^d the dissipative parts of the stress and internal remodeling action, respectively, the following equality must be satisfied for any actual stretching velocity $\dot{\lambda} = \dot{x}/x_{\text{ref}}$ and remodeling velocity $\dot{x}_r/x_r$:

$$\dot{\psi} + \underbrace{\sigma^d \cdot \dot{\lambda} + a^d \cdot \frac{\dot{x}_r}{x_r}}_{\text{dissipated power} \geq 0} = \underbrace{\sigma \cdot \dot{\lambda} + a^i \cdot \frac{\dot{x}_r}{x_r}}_{\text{internal power}} , \tag{17}$$

with the requirement that the dissipated power be always semi-definite positive. It is worth noting that Eq. (17) involves actual powers while Eq. (13) involves virtual powers. We assume that the dissipation component of the stress is zero, that is $\sigma^d = 0$. We also assume that there exists a purely elastic free energy ψ_r per unit rest length that depends on λ_e such that

$$\psi(\lambda_r, \lambda_e) = \lambda_r \, \psi_r(\lambda_e) . \tag{18}$$

Here, λ_r represents the (1D) Jacobian of the map from x_{ref} to x_r accounting for the change of density. Note that $\psi_r(1) = 0$ when $\lambda_e = 1$.

To exploit the consequences of Eq. (17), we must evaluate the energy rate $\dot{\psi}$. By using the formula

$$\dot{\lambda}_e = \frac{\dot{\lambda}}{\lambda_r} - \lambda_e \frac{\dot{\lambda}_r}{\lambda_r} , \tag{19}$$

we have that the energy rate has the form:

$$\dot{\psi} = \psi_r' \, \dot{\lambda} + \lambda_r \, (\psi_r - \lambda_e \, \psi_r') \, \frac{\dot{\lambda}_r}{\lambda_r} . \tag{20}$$

The second term on the right-hand side involves the Eshelby-like term e, introduced in Eq. $(3)_2$:

$$e = \hat{e}(\lambda_e) = \psi_r(\lambda_e) - \lambda_e \, \psi_r'(\lambda_e) . \tag{21}$$

Since $\dot{\lambda}_r/\lambda_r = \dot{x}_r/x_r$, replacing Eq. (20) in Eq. (17) yields for any $\dot{\lambda}$ and $\dot{x}_r/x_r$:

$$(\psi_r' - \sigma) \cdot \dot{\lambda} + (\lambda_r \, e + a^d - a^i) \cdot \frac{\dot{x}_r}{x_r} = 0 , \quad \forall \, \dot{\lambda} , \frac{\dot{x}_r}{x_r} . \tag{22}$$

The constitutive prescription for σ follows from the above equation and is already presented in Eq. (5). Similarly, the constitutive prescription for a^i

$$a^i = \lambda_r \, e + a^d . \tag{23}$$

The constitutive equation for a^d remains to be specified under the requirement that the dissipated power be always semi-definite positive for any $\dot{x}_r/x_r$:

$$a^d \cdot \frac{\dot{x}_r}{x_r} \geq 0 . \tag{24}$$

The simplest assumption is the following:

$$a^d = \frac{1}{m} \frac{\dot{x}_r}{x_r} , \tag{25}$$

where the mobility $m > 0$ has been presented and discussed in Section 3.1. By considering the above results, we can rewrite the balance Eqs. (16) as follows

$$\sigma = f , \quad \frac{\dot{x}_r}{x_r} = m \, (a - \lambda_r \, e) . \tag{26}$$

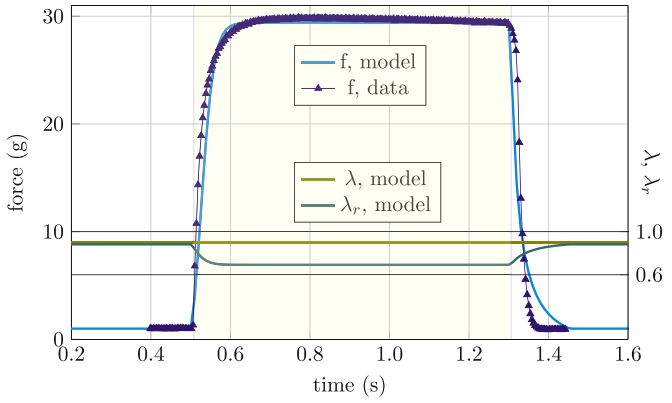

Fig. 8. Isometric contraction at $f_r = 150$ Hz. Experimental data (blue triangles) and model results (solid blue line) of force versus time. Model results of λ (light green line) and λ_r (dark green line) versus time. The shaded yellow region denotes the activation time interval. The two horizontal black thin lines represent the lower and upper bounds for λ_r which are related to the lower and upper bounds of x_r as defined in Fig. 3. Force is shown on left y-axis and λ and λ_r are on right y-axis. (For interpretation of the references to colour in this figure legend, the reader is referred to the web version of this article.)

These equations are equal to Eqs. (3).

4. Results and discussion

The modeling predictions have been compared to the experimental data that were obtained by testing the EDL of a mouse in isometric and isotonic contractions as described in Section 2, by tuning the values of the parameters κ, $\bar{m}$, and $\bar{a}$.

4.1. Isometric contractions

We evaluate the model by comparing the results of Eqns. (11) to the isometric data shown in Fig. 1. Toward this end, we consider a muscle of fixed length $\bar{x} = 0.9\, x_{\text{ref}}$, with $x_{\text{ref}} = 12.8$ mm, with $t_{\text{on}} = 0.47$ s, and $t_{\text{off}} = t_{\text{on}} + 0.84$ s. As in the experiments, in the model we assume that the muscle is pre-loaded at 1 g by assigning the pre-stretch $\varepsilon = 0.25$ mm (see Eq. $(11)_4$).

We solve Eqs. (11) for three different stimuli. For a frequency $f_r = 150$ Hz, we use a piecewise constant activation $a(t) = \bar{a}\, sh(t)$. For $f_r = 50$ Hz, that is when the frequency is low enough that the muscle response exhibits periodic oscillations, we use the piecewise oscillatory activation $a(t) = \bar{a}\, sp(t)$. Finally, to simulate the muscle response to a twitch, we use the piecewise oscillatory activation $a(t) = \bar{a}\, sp(t)$ with just one pulse.

The results of the isometric contractions are shown in Figs. 8–10, together with the data already shown in Fig. 1. Figs. 8–10 show the force, length (which is a horizontal line since the contraction is isometric), and rest length versus time. The force measured from the experiments is compared to the model results.

It is important to note that we are using a coarse-grained model of the muscle and many fine details such as the spreading of the activation potential or the number of motor units which are recruited upon activation are all subsumed in the three model parameters, namely κ, $\bar{m}$, and $\bar{a}$. We assumed that the value of κ, which defines the elastic properties of the muscle, does not change in different experiments such as the isometric and the isotonic ones but we tuned the other two parameters to reproduce the experimental data. For the isometric data, we used the parameter values listed in Table 1.

We note that, for the isometric experiments, the mobility $\bar{m}$ is low at $f_r = 150$ Hz and then increases as the frequency decreases; this reflects the fact that the muscle response becomes faster when tetanus is not developed and is the fastest when the stimulus is a

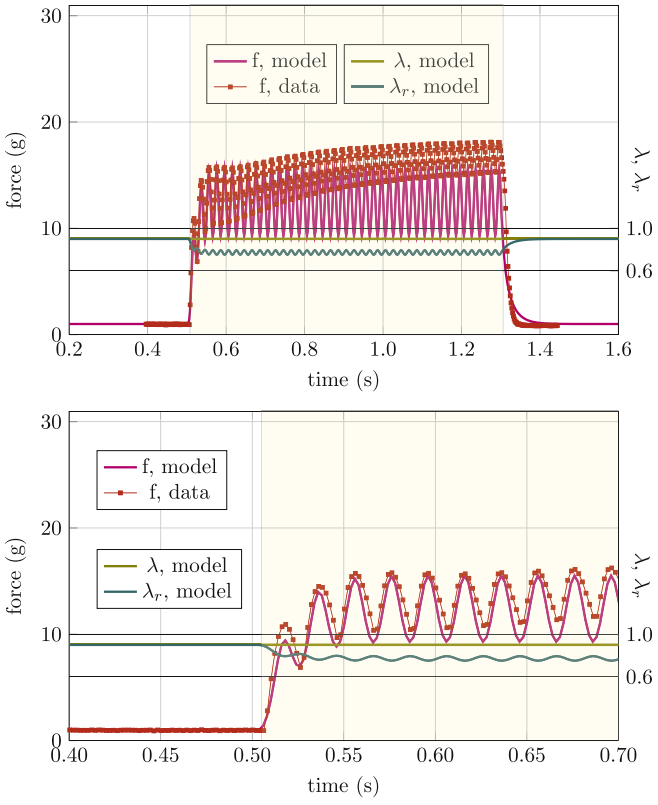

Fig. 9. Isometric contraction at $f_r = 50$ Hz. Top panel: Experimental data (red squares) and model results (solid red line) of force versus time. Model results of λ (dark green line) and λ_r (light green line) versus time. Bottom panel: Zoomed in view of the top panel up to 0.7 s. The shaded yellow region denotes the activation time interval. The two horizontal black thin lines represent the lower and upper bounds for λ_r which are related to the lower and upper bounds of x_r as defined in Fig. 3. Force is shown on left y-axis and λ and λ_r are on right y-axis. (For interpretation of the references to colour in this figure legend, the reader is referred to the web version of this article.)

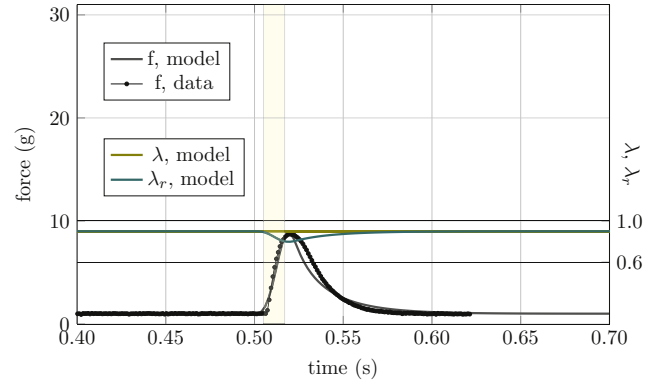

Fig. 10. Isometric contraction at single twitch. Experimental data (black dots) and model results (solid black line) of force versus time. Model results of λ (dark green line) and λ_r (light green line) versus time. The shaded yellow region denotes the activation time interval. The two horizontal black thin lines represent the lower and upper bounds for λ_r which are related to the lower and upper bounds of x_r as defined in Fig. 3. Force is shown on left y-axis and λ and λ_r are on right y-axis. (For interpretation of the references to colour in this figure legend, the reader is referred to the web version of this article.)

Table 1
Parameter values for isometric contractions.

Field	$f_r = 150$ Hz	$f_r = 50$ Hz	single twitch
κ (g)	6	6	6
$\bar{m}$ ($g^{-1}s^{-1}$)	0.33	0.95	1
$\bar{a}$ (g)	−24.1	−19	−15

Table 2
Experimental times.

Parameter	$\bar{f} = 1.58$ g	$\bar{f} = 7.2$ g	$\bar{f} = 21.2$ g
t_{on} (s)	0.290	0.290	0.300
t_{off} (s)	0.800	0.800	0.810
$\bar{t}_{off}$ (s)	0.885	0.898	0.863

twitch. Conversely, the activation $\bar{a}$ is high at $f_r = 150$ Hz and then decreases as the frequency decreases; this is due to the fact that at $f_r = 150$ Hz we have the maximum force production, that is, the maximum number of recruited motor-units, and hence a higher activation.

In order to keep the model as simple as possible, we assume that the value of the parameters do not change during each experiment. However, this assumption could be relaxed by choosing parameters which are a function of time. Under this assumption, one can potentially better reproduce the experimental results. For example, in Fig. 9 (top), it can be observed that the experimentally measured oscillating force drifts away towards large average values, a phenomenon better appreciated in Fig. 2 where only the experimental data are presented; this phenomenon can likely be captured by choosing $\bar{m}$ and $\bar{a}$ that vary with time.

One relevant characteristic of the proposed model is that it provides the rest length x_r as function of time. Although the experiments do not provide data on how x_r changes over time, the force versus time data offer some indirect measurements of the change in x_r since x_r is related to force production by Eq. $(11)_1$. As the frequency decreases, the change in rest length (the contraction) and the force decrease.

4.2. Isotonic contractions

We compare the solutions of system (12) to the isotonic data shown in Fig. 2. Toward this end, we use the piecewise constant activation $a(t) = \bar{a}\, sh(t)$ with the activation times t_{on} and t_{off} reported in Table 2. Then we define a force history $f(t)$, as controlled in the experiments, by using the complementary error function erfc as follows:

$$f(t) = f_o + \left(\bar{f} - f_o\right) sf(t)\,, \tag{27}$$

$$sf(t) = \frac{1}{2}\,\mathrm{erfc}\left(\frac{-t + (\bar{t}_{on} + \delta_t)}{\sqrt{2}\,\delta_f}\right) \tag{28}$$

$$-\frac{1}{2}\,\mathrm{erfc}\left(\frac{-t + (\bar{t}_{off} - \delta_t)}{\sqrt{2}\,\delta_f}\right), \tag{29}$$

where $f_o = 1$ g represents a pre-load, and $\bar{f}$ is the value of $f(t)$ at the plateau. Moreover, $\delta_t = 0.02$ and $\delta_f = 0.08$ are tuned to reproduce the experimental force history. We note that the times $\bar{t}_{on}$ and $\bar{t}_{off}$ in $sf(t)$ may be different to the ones appearing in $sh(t)$.

We solve Eqs. (12) for three isotonic contractions under the forces $\bar{f} = 1.58$ g, $\bar{f} = 7.2$ g, and $\bar{f} = 21.2$ g and $\varepsilon = 0$. For each contraction, the times t_{on}, t_{off}, and $\bar{t}_{off}$ are listed in Table 2 and $\bar{t}_{on} = t_{on}$. The goal is to determine the couple (x, x_r) from the model and compare the stretch λ over time with the corresponding stretch $\bar{x}/x_{ref} + s(t)/x_{ref}$ of the muscle that is computed from

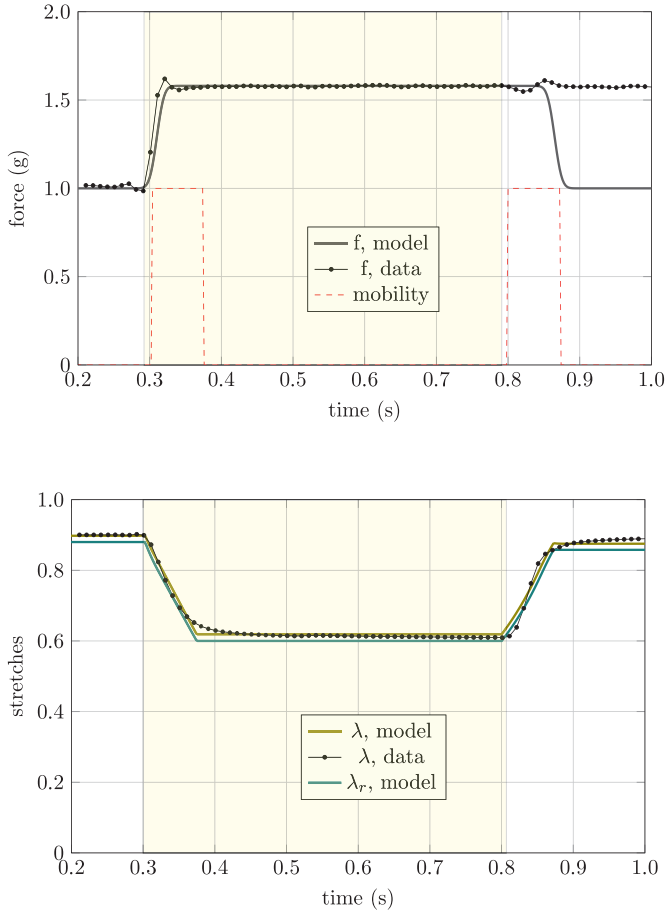

Fig. 11. Isotonic contraction at $\bar{f} = 1.58$ g. Experimental data (black dots) and model results (solid black line) of force (top) and stretch λ (bottom) versus time. Model results (green line) for λ_r (bottom). The mobility switch is shown too (dashed red line) (top). The shaded yellow region denotes the activation time interval. (For interpretation of the references to colour in this figure legend, the reader is referred to the web version of this article.)

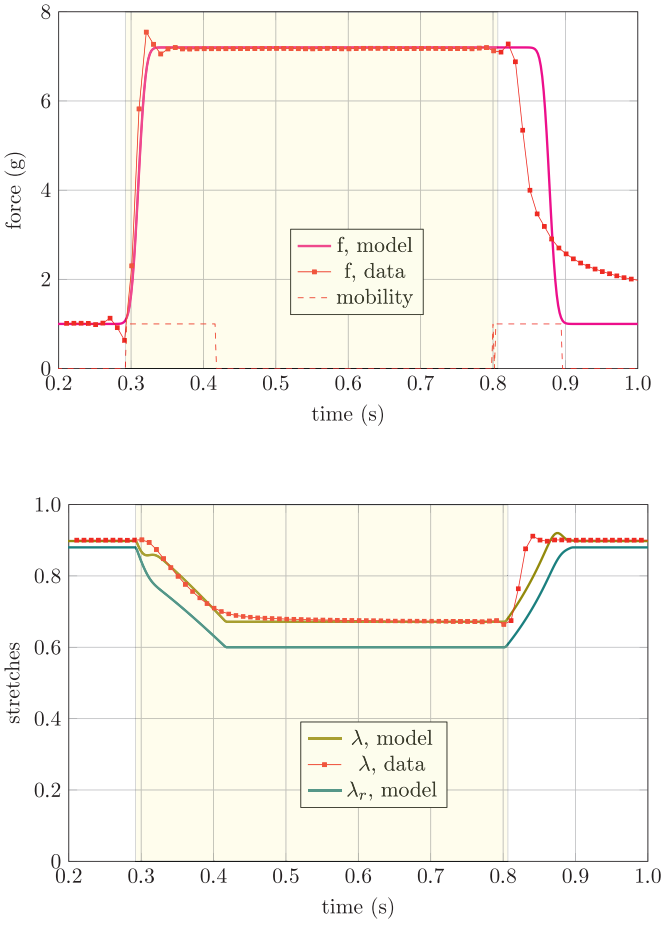

Fig. 12. Isotonic contraction at $\bar{f} = 7.2$ g. Experimental data (red squares) and model results (solid red line) of force (top) and stretch λ (bottom) versus time. Model results (green line) for λ_r (bottom). The mobility switch is shown too (dashed red line) (top). The shaded yellow region denotes the activation time interval. (For interpretation of the references to colour in this figure legend, the reader is referred to the web version of this article.)

Table 3
Parameter values for isotonic contractions.

Parameter	$\bar{f} = 1.58$ g	$\bar{f} = 7.2$ g	$\bar{f} = 21.2$ g
κ (g)	6	6	6
$\bar{m}$ ($g^{-1}s^{-1}$)	4.5	0.9	0.6
$\bar{a}$ (g)	−2.3	−8.15	−17.53

the shortening $s(t)$ measured in the experiments (see Fig. 2 (bottom)).

The model results for the isotonic tests are shown in Figs. 11–13, together with the data already shown in Fig. 2. Each figure presents two subfigures: the top one shows experimental and model results for force over time and the mobility switch $m_\sigma(\sigma - \sigma_t)\, m_a(x_r, a - \lambda_r e)/\bar{m}$; the bottom one shows experimental and model results for λ and λ_r over time. For the isotonic experiments, we used the values listed in Table 3. Here, the same remarks done for the isometric tests hold; we note that the higher is the force production, the higher is the activation $\bar{a}$ and the smaller is the mobility $\bar{m}$.

The first isotonic contraction is performed at $\bar{f} = 1.58$ g, a very low force that corresponds to $\sim 5\%$ of the maximum tetanic force and is only 0.55 g higher than the pre-load $\sigma_t = 1$ g. Muscle shortening is the largest and the shortening rate is the highest among the three isotonic experiments (Fig. 2). We note that, in this experiment, the force is maintained constant even after the initial length has been recovered at $t > 0.85$ s. A post-load that is slightly higher than the pre-load is seen also in the other experiments, but it is less noticeable as $\bar{f}$ becomes larger than the post-load. A possible cause could be the increased length of the muscle yielding a post-load higher that the pre-load.

The agreement between the experiments and model is satisfactory (Fig. 11). For simplicity, we neglect the description of the post-load (after $t \simeq 0.85$ s the measured force stays at its value of $\simeq 1.5$ g, while the simulated force goes back to 1 g), and we simulate a force history that returns to the pre-load value after the initial λ is recovered. However, we could model the post-load behavior of the muscle, as done for the pre-load, by defining a mobility function m that depends also on the post-load. The second isotonic contraction is performed at $\bar{f} = 7.2$ g, which corresponds to $\sim 25\%$ of the maximum tetanic force. Both the muscle shortening and shortening rate are smaller than those recorded in the previous isotonic experiment at $\bar{f} = 1.58$ g (Fig. 2). The agreement between experiments and model is satisfactory (Fig. 12), especially during the loading phase and the constant plateau; the post-load phase is not reproduced with the same accuracy. We note that force decay and the stretch recovery are different between model and experiments due again to the presence of a ~ 2 g post-load.

The third and last isotonic contraction is performed at $\bar{f} = 21.2$ g, a high force for the tested muscle, which corresponds to $\sim 75\%$ of the maximum tetanic force. Both muscle shortening and short-

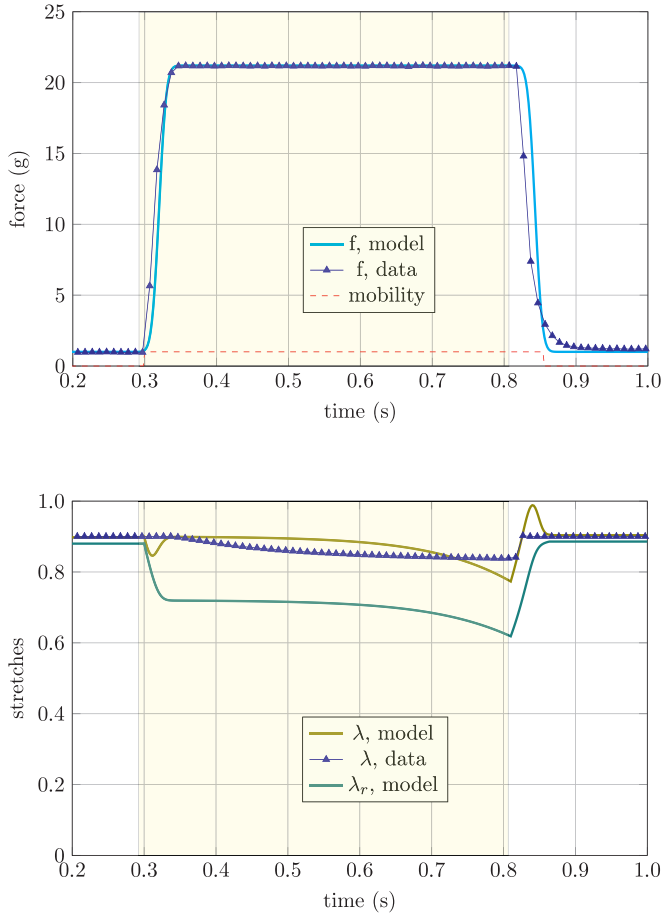

Fig. 13. Isotonic contraction at $\bar{f} = 21.2$ g. Experimental data (blue triangles) and model results (solid blue line) of force (top) and stretch λ (bottom) versus time. Model results (green line) for λ_r (bottom). The mobility switch is shown too (dashed red line) (top). The shaded yellow region denotes the activation time interval. (For interpretation of the references to colour in this figure legend, the reader is referred to the web version of this article.)

ening rate are very small (Fig. 2). The agreement between experiments and model is quite satisfactory for the force history, but not as good for the stretch history (Fig. 13). We note that the curve describing $\lambda(t)$ has two bumps at t_{on} and t_{off}. These are due to the inherent numerical difficulties in integrating the system of equations that results in this case. Moreover, while the muscle shortening is slowly decreasing for almost the entire activation time, the stretch predicted by the model reaches a plateau value much faster. As mentioned earlier, the model could capture this behavior by assuming a time varying $\bar{m}$ for the mobility function.

5. Conclusions

We present a mathematical model for muscle mechanics that captures experimental observations made during isometric and isotonic tests. In the proposed model, although we gloss over the details of the microscopic processes that lead to muscle contraction, we account for the macroscopic mechanical effect of the chemical/electrical input. The model is derived within the context of a well-known rational mechanics framework that invokes the *principle of power balance* and the *dissipation principle*. It is tested under both isometric and isotonic conditions by tuning the values of three model parameters in order to match the experimental data. A key feature of the model is the prediction of the muscle rest length, a quantity that cannot be experimentally measured.

Due to its simplicity, this one-dimensional model of muscle contraction can be easily embedded into a three-dimensional model of muscle tissues. This can be done by assuming that the active mechanics of muscle fibers that mainly comprise the tissue can be described by the proposed model. This extended three-dimensional model could then be implemented into finite element codes for studying the role of passive and active muscle mechanics in many natural phenomena (e.g., fish swimming (Curatolo and Teresi, 2016; Lucantonio et al., 2014; Nawroth et al., 2012)) and many muscular diseases (e.g., muscular dystrophy (Virgilio et al., 2015)).

Conflict of Interest

The authors have no conflict of interest.

Acknowledgements

This work was supported by Sapienza - Università di Roma through the Sapienza Mobility Grant (prot. 0047591) and NSF award number 1511603. L.T. acknowledges the Italian Group of Mathematical Physics (GNFM - INdAM).

References

Ambrosi, D., Arioli, G., Nobile, F., Quarteroni, A., 2011. Electromechanical coupling in cardiac dynamics: the active strain approach. SIAM J. Appl. Math. 71, 605–621.
Ambrosi, D., Guana, F., 2007. Stress-modulated growth. Math. Mech. Solids 12, 319–342.
Chen, H., Luo, T., Zhao, X., Lu, X., Huo, Y., Kassab, G.S., 2013. Microstructural constitutive model of active coronary media. Biomaterials 34, 7575–7583.
Cherubini, C., Filippi, S., Nardinocchi, P., Teresi, L., 2008. An electromechanical model of cardiac tissue: constitutive issues and electrophysiological effects. Prog. Biophys. Mol. Biol. 97, 562–573.
Coleman, B.D., Noll, W., 1963. The thermodynamics of elastic materials with heat conduction and viscosity. Arch. Ration. Mech. Anal. 13, 167–178.
Curatolo, M., Teresi, L., 2016. Modeling and simulation of fish swimming with active muscles. J. Theor. Biol. 409, 18–26.
DiCarlo, A., Quiligotti, S., 2002. Growth and balance. Mech. Res. Commun. 29, 449–456.
Dickinson, M.H., Farley, C.T., Full, R.J., Koehl, M., Kram, R., Lehman, S., 2000. How animals move: an integrative view. Science 288, 100–106.
Dillon, P.F., Aksoy, M.O., Driska, S.P., Murphy, R.A., 1981. Myosin phosphorylation and the cross-bridge cycle in arterial smooth muscle. Science 211, 495–497.
Germain, P., 1972. Sur lapplication de la méthode des puissances virtuelles en mécanique des milieux continus. C. R.Acad. Sci. 274, 1051–1055.
Göktepe, S., Menzel, A., Kuhl, E., 2014. The generalized hill model: a kinematic approach towards active muscle contraction. J. Mech. Phys. Solids 72, 20–39.
Gurtin, M.E., 2008. Configurational Forces as Basic Concepts of Continuum Physics, volume 137. Springer Science & Business Media.
Hill, A.V., 1938. The heat of shortening and the dynamic constants of muscle. Proc. R. Soc. London B: Biological Sciences 126, 136–195.
Hunter, P.J., McCulloch, A.D., Keurs, H.E.D.J.T., 1998. Modelling the mechanical properties of cardiac muscle. Prog. Biophys. Mol. Biol. 69, 289–331.
Keurs, H.E.D.J.T., Rijnsburger, W.H., Heuningen, R.V., Nagelsmit, M.J., 1980. Tension development and sarcomere length in rat cardiac trabeculae: evidence of length-dependent activation. In: Cardiac Dynamics. Springer, pp. 25–36.
Lucantonio, A., Nardinocchi, P., Pezzulla, M., Teresi, L., 2014. Multiphysics of bio-hybrid systems: shape control and electro-induced motion. Smart Mater. Struct. 23 (4), 045043.
Maugin, G.A., 1993. Material Inhomogeneities in Elasticity. CRC.
Minozzi, M., Nardinocchi, P., Teresi, L., Varano, V., 2015. Growth-induced compatible strains. Math. Mech. Solids doi:10.1177/1081286515570510.
Murtada, S., Holzapfel, G.A., 2014. Investigating the role of smooth muscle cells in large elastic arteries: a finite element analysis. J. Theor. Biol. 358, 1–10.
Murtada, S.C., Arner, A., Holzapfel, G.A., 2012. Experiments and mechanochemical modeling of smooth muscle contraction: significance of filament overlap. J. Theor. Biol. 297, 176–186.
Nardinocchi, P., Teresi, L., 2006. Stress driven remodeling of living tissues. In: Comsol Multiphysics Conference 2005: Proceedings and User Presentations CD.
Nardinocchi, P., Teresi, L., 2007. On the active response of soft living tissues. J. Elast. 88, 27–39.
Nardinocchi, P., Teresi, L., 2013. Electromechanical modeling of anisotropic cardiac tissues. Math. Mech. Solids 18, 576–591.
Nawroth, J.C., Lee, H., Feinberg, A.W., Ripplinger, C.M., McCain, M.L., Grosberg, A., Dabiri, J.O., Parker, K.K., 2012. A tissue-engineered jellyfish with biomimetic propulsion. Nat. Biotechnol. 30, 792–797.
Quiat, D., Voelker, K.A., Pei, J., Grishin, N.V., Grange, R.W., Bassel-Duby, R., Olson, E.N., 2011. Concerted regulation of myofiber-specific gene expression and

muscle performance by the transcriptional repressor sox6. Proc. Natl. Acad. Sci. 108, 10196–10201.
Rodriguez, E., Hoger, A., McCulloch, A., 1994. Stress dependent finite growth in soft elastic tissues. J. Biomech. 27, 455–464.
Sharifimajd, B., Stålhand, J., 2014. A continuum model for excitation–contraction of smooth muscle under finite deformations. J. Theor. Biol. 355, 1–9.
Sperringer, J.E., Grange, R.W., 2016. In vitro assays to determine skeletal muscle physiologic function. In: Skeletal Muscle Regeneration in the Mouse: Methods and Protocols, pp. 271–291.
Stålhand, J., Klarbring, A., Holzapfel, G.A., 2008. Smooth muscle contraction: mechanochemical formulation for homogeneous finite strains. Prog. Biophys. Mol. Biol. 96, 465–481.
Stålhand, J., Klarbring, A., Holzapfel, G.A., 2011. A mechanochemical 3D continuum model for smooth muscle contraction under finite strains. J. Theor. Biol. 268, 120–130.
Stålhand, J., McMeeking, R.M., Holzapfel, G.A., 2016. On the thermodynamics of smooth muscle contraction. J. Mech. Phys. Solids.
Tan, T., De Vita, R., 2015. A structural constitutive model for smooth muscle contraction in biological tissues. Int. J. Non Linear Mech. 75, 46–53.
Truesdell, C., Noll, W., 1965. The non-linear field theories of mechanics. Handbuch der Physik, III/3. Berlin-Heidelberg-New York: Springer.
Virgilio, K.M., Martin, K.S., Peirce, S.M., Blemker, S.S., 2015. Multiscale models of skeletal muscle reveal the complex effects of muscular dystrophy on tissue mechanics and damage susceptibility. Interface Focus 5, 20140080.
Wolff, A.V., Niday, A.K., Voelker, K.A., Call, J.A., Evans, N.P., Granata, K.P., Grange, R.W., 2006. Passive mechanical properties of maturing extensor digitorum longus are not affected by lack of dystrophin. Muscle Nerve 34, 304–312.